Sub-diffraction resolution pump-probe microscopy with shot-noise limited sensitivity using laser diodes

Jun Miyazaki,[1,2] Hiromichi Tsurui,[3] Akiko Hayashi-Takagi,[2,4] Haruo Kasai[2,4] and Takayoshi Kobayashi[1, 2, 5, 6,*]

[1] *Advanced Ultrafast Laser Research Center, The University of Electro-Communications, 1-5-1 Chofugaoka, Chofu, Tokyo, 182-8585, Japan*

[2] *JST, CREST, K' Gobancho, 7, Gobancho, Chiyoda-ku, Tokyo 102-0076, Japan*

[3] *Department of Pathology, Juntendo University School of Medicine, 2-1-1, Hongo, Bunkyo-ku,Tokyo 113-8421, Japan*

[4] *Department of Structural Physiology, Graduate School of Medicine, The University of Tokyo, 7-3-1, Hongo, Bunkyoku, Tokyo, 113-0033, Japan.*

[5] *Department of Electrophysics, National Chiao-Tung University, Hsinchu 300, Taiwan*

[6] *Institute of Laser Engineering, Osaka University, 2-6 Yamada-oka, Suita, Osaka 565-0971, Japan*

[*] *kobayashi@isl.uec.ac.jp*

Abstract: We demonstrate the use of intensity-modulated laser diodes to implement pump-probe microscopy and achieved sub-diffraction resolution imaging with shot-noise limited sensitivity with a scheme of balanced detection. This technique has several applications for various types of induced transmission change, including excited-state absorption, ground state absorption bleaching and stimulated emission. By using our technique, biological imaging of mouse T cells and the axons of neurons in the cerebral cortex was demonstrated.

OCIS codes: (180.0180) Microscopy; (140.2020) Diode lasers; (100.6640) Superresolution.

References and links

1. D. Fu, T. Ye, T. E. Matthews, G. Yurtsever, and W. S. Warren, "Two-color, two-photon, and excited-state absorption microscopy," J. Biomed. Opt. **12**(5), 054004 (2007).
2. D. Fu, T. Ye, T. E. Matthews, B. J. Chen, G. Yurtserver, and W. S. Warren, "High-resolution in vivo imaging of blood vessels without labeling," Opt. Lett. **32**(18), 2641–2643 (2007).
3. T. Chen, F. Lu, A. M. Streets, P. Fei, J. Quan, and Y. Huang, "Optical imaging of non-fluorescent nanodiamonds in live cells using transient absorption microscopy," Nanoscale **5**(11), 4701–4705 (2013).
4. S. S. Chong, W. Min, and X. S. Xie, "Ground-state depletion microscopy: Detection sensitivity of single-molecule optical absorption at room temperature," J. Phys. Chem. Lett. **1**(23), 3316–3322 (2010).
5. W. Min, S. Lu, S. Chong, R. Roy, G. R. Holtom, and X. S. Xie, "Imaging chromophores with undetectable fluorescence by stimulated emission microscopy," Nature **461**(7267), 1105–1109 (2009).
6. T. Dellwig, P. Y. Lin, and F. J. Kao, "Long-distance fluorescence lifetime imaging using stimulated emission," J. Biomed. Opt. **17**(1), 011009 (2012).
7. C. Y. Dong, C. Buehler, P. T. So, T. French, and E. Gratton, "Implementation of intensity-modulated laser diodes in time-resolved, pump-probe fluorescence microscopy," Appl. Opt. **40**(7), 1109–1115 (2001).
8. C. Y. Dong, P. T. C. So, T. French, and E. Gratton, "Fluorescence lifetime imaging by asynchronous pump-probe microscopy," Biophys. J. **69**(6), 2234–2242 (1995).
9. T. Chen, F. Lu, A. M. Streets, P. Fei, J. M. Quan, and Y. Y. Huang, "Optical imaging of non-fluorescent nanodiamonds in live cells using transient absorption microscopy," Nanoscale **5**(11), 4701–4705 (2013).
10. L. Tong, Y. Liu, B. D. Dolash, Y. Jung, M. N. Slipchenko, D. E. Bergstrom, and J. X. Cheng, "Label-free imaging of semiconducting and metallic carbon nanotubes in cells and mice using transient absorption microscopy," Nat. Nanotechnol. **7**(1), 56–61 (2011).
11. T. Ye, D. Fu, and W. S. Warren, "Nonlinear absorption microscopy," Photochem. Photobiol. **85**(3), 631–645 (2009).
12. D. Fu, T. Ye, T. E. Matthews, J. Grichnik, L. Hong, J. D. Simon, and W. S. Warren, "Probing skin pigmentation changes with transient absorption imaging of eumelanin and pheomelanin," J. Biomed. Opt. **13**(5), 054036 (2008).
13. T. E. Matthews, I. R. Piletic, M. A. Selim, M. J. Simpson, and W. S. Warren, "Pump-probe imaging differentiates melanoma from melanocytic nevi," Sci. Transl. Med. **3**(71), 71ra15 (2011).

#206121 - $15.00 USD Received 7 Feb 2014; revised 26 Mar 2014; accepted 1 Apr 2014; published 7 Apr 2014

14. M. J. Simpson, K. E. Glass, J. W. Wilson, P. R. Wilby, J. D. Simon, and W. S. Warren, "Pump-probe microscopic imaging of Jurassic-aged eumelanin," J Phys Chem Lett **4**(11), 1924–1927 (2013).
15. L. Wei and W. Min, "Pump-probe optical microscopy for imaging nonfluorescent chromophores," Anal. Bioanal. Chem. **403**(8), 2197–2202 (2012).
16. M. Celebrano, P. Kukura, A. Renn, and V. Sandoghdar, "Single-molecule imaging by optical absorption," Nat. Photonics **5**(2), 95–98 (2011).
17. P. Kukura, M. Celebrano, A. Renn, and V. Sandoghdar, "Single-Molecule Sensitivity in Optical Absorption at Room Temperature," J. Phys. Chem. Lett. **1**(23), 3323–3327 (2010).
18. J. R. Lakowicz, *Topics in Fluorescence Spectroscopy, Vol 5: Nonlinear and Two-Photon Induced Fluorescence* (Springer, 1997), Vol. 5.
19. A. Gaiduk, M. Yorulmaz, P. V. Ruijgrok, and M. Orrit, "Room-temperature detection of a single molecule's absorption by photothermal contrast," Science **330**(6002), 353–356 (2010).
20. S. Berciaud, D. Lasne, G. A. Blab, L. Cognet, and B. Lounis, "Photothermal heterodyne imaging of individual metallic nanoparticles: Theory versus experiment," Phys. Rev. B **73**(4), 045424 (2006).
21. K. Uchiyama, A. Hibara, H. Kimura, T. Sawada, and T. Kitamori, "Thermal lens microscope," Jpn. J. Appl. Phys. **39**(Part 1, No. 9A), 5316–5322 (2000).
22. A. Avramescu, T. Lermer, J. Müller, C. Eichler, G. Bruederl, M. Sabathil, S. Lutgen, and U. Strauss, "True Green Laser Diodes at 524 nm with 50 mW Continuous Wave Output Power onc-Plane GaN," Appl. Phys. Express **3**(6), 061003 (2010).
23. S. Takagi, Y. Enya, T. Kyono, M. Adachi, Y. Yoshizumi, T. Sumitomo, Y. Yamanaka, T. Kumano, S. Tokuyama, K. Sumiyoshi, N. Saga, M. Ueno, K. Katayama, T. Ikegami, T. Nakamura, K. Yanashima, H. Nakajima, K. Tasai, K. Naganuma, N. Fuutagawa, Y. Takiguchi, T. Hamaguchi, and M. Ikeda, "High-Power (over 100 mW) Green Laser Diodes on Semipolar {2021} GaN Substrates Operating at Wavelengths beyond 530 nm," Appl. Phys. Express **5**(8), 082102 (2012).
24. J. Kasai, R. Akimoto, T. Hasama, H. Ishikawa, S. Fujisaki, S. Tanaka, and S. Tsuji, "Green-to-yellow continuous-wave operation of BeZnCdSe quantum-well laser diodes at room temperature," Appl. Phys. Express **4**(8), 082102 (2011).

1. Introduction

In pump-probe experiments, pump light promotes molecules to an allowed excited state, which in turn induces changes in probe transmissivity via excited-state absorption [1–3], ground state absorption bleaching [4], and stimulated emission [5–8]. This method has recently been used in optical microscopy to visualize the structure of biological tissues and to carry out functional analysis, such as the imaging of ñuorophores that have short-lived excited states [1, 4, 5, 9, 10], the label-free biological imaging of red blood cells [2, 11], analysis of melamine pigments and melanoma diagnosis [12–14].

The relative change in the probe intensity in pump-probe microscopy is estimated to be no more than 10^{-7} - 10^{-6} from the absorption cross section (typically 10^{-16}-10^{-15} cm^2) and focus spot size for a single molecule located in the focal volume of an objective lens [15]. Therefore, extremely stable lasers with special additional features are necessary to detect such weak signals, particularly as the laser noise interferes with their detection. The recent development of pump-probe microscopy has been carried out typically by using mode-locked femtosecond pulse laser oscillator with high repetition rates and high-frequency lock-in detection schemes to avoid laser-intensity fluctuation, which is larger at lower frequencies. Xie and associates have performed stimulated emission microscopy by employing two optical parametric oscillators (OPOs) pumped by a high-intensity Ti:sapphire or Yb mode-locked laser to obtain wavelength-tunable and synchronous pump and probe pulse trains [5]. However, these mode-locked laser-based systems with OPOs are very expensive and complex.

In this study, using intensity modulated continuous wave laser diodes (LDs) with a balanced detection scheme [16, 17], we accomplished sub-diffraction resolution pump-probe imaging with shot-noise limited sensitivity. We also demonstrated the use of this method for the biological imaging of mouse T cells and the axons of neurons in the cerebral cortex.

2. Experiment

2.1 Principe of pump-probe microscopy using intensity modulated lasers

The principle of pump-probe microscopy using intensity modulated continuous wave laser is illustrated in Fig. 1. The probe and pump-beam intensities were set to frequencies of ω_1 and

#206121 - $15.00 USD Received 7 Feb 2014; revised 26 Mar 2014; accepted 1 Apr 2014; published 7 Apr 2014

ω_2, respectively. A beat signal at $|\omega_1 - \omega_2|$ is generated by the bilinear interaction of the pump field and the probe field in the sample. We used a lock-in technique to detect the signal, and the lock-in amplifier was referenced to the beat frequency. By changing the modulation frequencies (ω_1 and ω_2) while holding (or maintaining) $|\omega_1 - \omega_2|$ constant, this dual-modulation scheme has the potential to acquire time-resolved information without a high-speed detector [7].

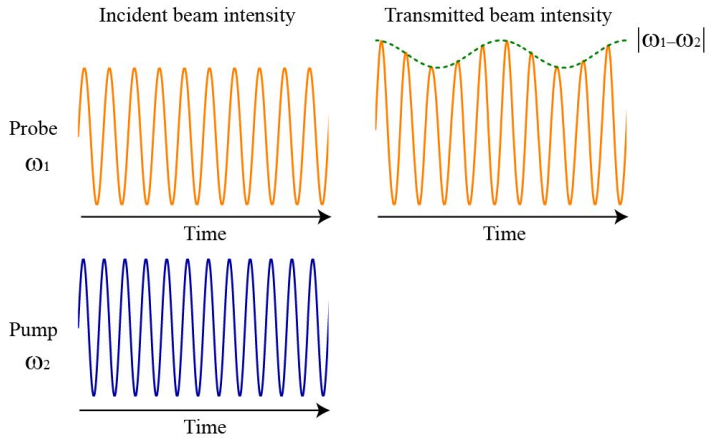

Fig. 1. Principle of pump-probe microscopy using intensity modulated continuous wave laser. The probe and pump beam intensities are modulated at ω_1 and ω_2. A beat signal at $|\omega_1 - \omega_2|$ is generated by the bilinear interactions at sample position and detected using a lock-in amplifier.

2.2 Experimental system

Our pump-probe microscopy system, which uses simple LDs and a balance detector, is illustrated in Fig. 2. Two laser diodes (Nichia NDS4216 and Mitsubishi ML101U29) were used for excitation at 488 nm and probing at 660 nm, respectively. Their output powers were 200 mW. A diode pumped solid state (DPSS) laser (Thorlabs, DJ525-40) with an output power of 40 mW was used as an alternative probe beam. The LDs and the DPSS were mounted on temperature-controlled laser-diode mounts (Thorlabs, TCLDM9 or LDM9T). Each beam was collimated through a spatial filter and the three beams were combined with dichroic beam-combining mirrors. All of the beams were linearly (vertically) polarized. A polarizing beam splitter (PBS) was used to direct the combined beam to the objective lens (Olympus: UPLSAPO 40X2 or UPLSAPO 100XO) with numerical apertures (NA) of 0.95 and 1.4. The beam size was adjusted to fill the back aperture of the objective lens. The sample position was raster-scanned using a three-axis positioning stage driven by piezo actuators (Thorlabs MAX311D). To evaluate the spatial resolution using a gold nanoparticle, we used a high-accuracy positioning stage (PI P-622.2) with a closed-loop resolution of 0.7 nm. A 1.4-NA oil immersion condenser lens (Olympus U-AAC) was used to collect the transmitted light. A narrowband filter matching the laser line was placed in front of the detector to filter out both the excitation beam and the fluorescence from the sample, so that only the probe beam was detected. An auto-balanced photoreceiver (New Focus, Nirvana) was used to cancel out the intensity-fluctuation noise of the probe laser. A beam splitter placed in front of the focusing lens reflected the probe beam, which was then directed to the reference port of the balanced detector through a multimode fiber. The output of the balanced detector can be expressed as $V_{out} = G\gamma\ [p_{sig} - g\ p_{ref}]$, where G and g are the trans-impedance gain of the detector and the reference-channel gain, respectively, γ is the photodiode sensitivity and $p_{sig(ref)}$ is the beam power incident on the signal (reference) photodiode. A neutral density filter was used to set the reference-beam intensity to about twice the probe intensity for optimal common-mode noise rejection. We also set up a fluorescence detection scheme,

#206121 - $15.00 USD Received 7 Feb 2014; revised 26 Mar 2014; accepted 1 Apr 2014; published 7 Apr 2014

wherein the fluorescence signal from the sample was detected by a photo-multiplier tube through the objective lens, a PBS and a multimode fiber with a core diameter of 100 μm.

A signal generator (Rigol DG4162) and an amplifier (Mini-circuit ZHL-6A +) were used to sinusoidally modulate the light intensity of each LD by adjusting the injection current from the kHz to the MHz range. The light intensity of the DPSS laser was externally modulated using an electro-optic modulator (EOM) (LINOS LM020). A lock-in amplifier (Signal Recovery 7270) was used to detect the pump-probe signal. The output of the balanced detector was connected to the lock-in amplifier through a low-pass filter (Mini-circuit LPF-B0R3). The reference signal for the lock-in amplifier was delivered from the two signal generators through a frequency mixer (Mini-circuit ZAD-1) and a low-pass filter (Mini-circuit LPF-B0R3). As it was crucial to avoid signal interference between the pump and the probe channels, we placed a 30-dB attenuator and an amplifier (Mini-circuit ZFL-500LN) between the signal generator and the frequency mixer. Furthermore, to reduce interference between the two channels due to electromagnetic (EM) waves, the LDs and the DPSS laser were placed in separate EM-shielding boxes.

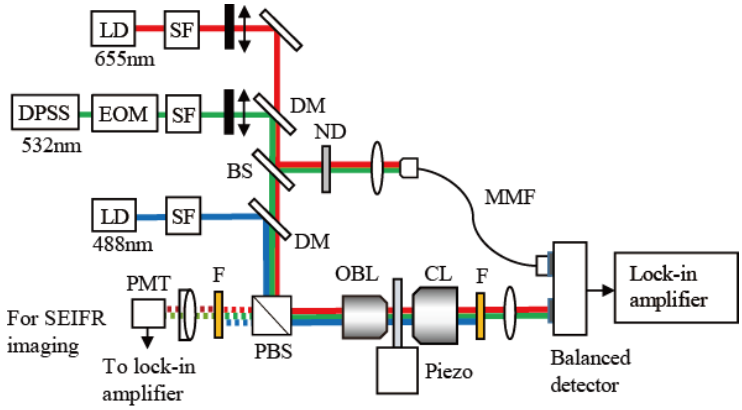

Fig. 2. Experimental setup of pump-probe microscopy using laser diodes. LD: laser diode, DPSS: diode pumped solid state laser, EOM: electro optical modulator, SF: spatial filter, DM: dichroic mirror, BS: beam splitter, ND: neutral density filter, PBS: polarization beam splitter, OBL: objective lens. CL: condenser lens, F: band pass filter, PMT: photomultiplier tube, MMF: multimode fiber. Either the 660 nm LD or the 532 nm DPSS was used as a probe light source.

2.3 Evaluation of the noise level and signal to noise ratio

Using this setup, we first examined the noise level, signal intensity and signal-to-noise ratio (SNR) to ascertain the optimal probe-beam power. Figure 3(a) shows the noise level of the lock-in signal as a function of p_{sig} (660-nm LD). When p_{sig} was below ~10^{-5} W, circuit noise was dominant, at the level of 1.2×10^{-7} $(V/\sqrt{Hz})$. After cancelling the laser-intensity fluctuation, we found the root mean square (RMS) of the noise of the lock-in signal to be close to the theoretical shot-noise level when p_{sig} = 10^{-5} - 10^{-4} W. Here, the shot-noise level was calculated using the equation $v_{shot} = G\sqrt{2q\gamma p_{sig}}$ $(V/\sqrt{Hz})$, where q is the elementary charge, G = 1 x 10^5 (V/A), and γ = 0.43 (A/W). When p_{sig} was larger than 10^{-4} W, the noise level seemed to deviate from the shot-noise level due to the residual laser noise; however, the laser noise was substantially reduced, showing a decrease of about 26-dB.

Figure 3(b) shows the typical lock-in signal and the signal-to-noise ratio (SNR) as functions of the power of the probe beam power p_{probe} incident on a sample. The sample was a thin film polymer doped with CdSe/ZnS quantum dots, which emit fluorescence with a peak at 650 nm. We used 488-nm and 660-nm LDs for the pump and the probe, respectively. The probe-laser wavelength was found to overlap the fluorescence spectrum of the quantum dots,

#206121 - $15.00 USD Received 7 Feb 2014; revised 26 Mar 2014; accepted 1 Apr 2014; published 7 Apr 2014

such that the main contributor to the pump-probe signal was considered to be the stimulated emission. The gain of signal intensity was found to saturate as p_{probe} increased up to ~100 μW. The maximum SNR was reached prior to signal saturation. Theoretical calculations using rate equations indicate that signal saturation occurs when k_{se} exceeds k_s in the limit of weak pump power. Here $k_{se} = \sigma_{se} p_{probe} / (h\nu_{probe} s)$ is the stimulated-emission rate; σ_{se} is the stimulated emission cross section; h is Plank's constant; and s is the beam waist at a focal point. k_s is the total decay rate of fluorescence radiative and nonradiative relaxations. The fluorescence lifetime of CdSe/ZnS was 13 ns, so the optimal value of p_{probe} that is close to saturation but not substantial saturation can be calculated as ~80 μW, by assuming $\sigma_{se} = 5 \times 10^{-16}$ cm^2 and $s = 5 \times 10^{-9}$ cm^2. This value is consistent with our experimental result, and at this laser power level, the SNR is mainly limited by shot noise. It is possible to reach this power level by LD, as the maximum output power is typically above 10 mW.

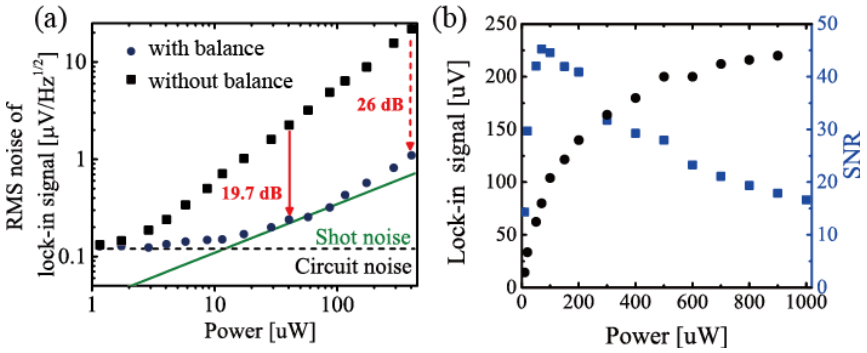

Fig. 3. Evaluation of noise level, signal intensity and signal-to-noise ratio (a). Noise level of the lock-in signal as a function of laser beam power incident on the detector. Circles and squares denote, respectively, lock-in signals that do or do not involve a balanced detection scheme. Solid and broken lines are the shot-noise level and circuit noise level, respectively. The modulation frequency of the beams was 3.0 MHz and the lock-in frequency was set at 100 kHz. (b). Lock-in signal (circles) and the signal to noise ratio (SNR) (squares) as a function of probe beam power at the sample position. The pump beam power was set at 20 μW. The modulation frequency of the probe and pump beams were 3.0 and 3.1 MHz, respectively.

2.4 Enhancement of the spatial resolution

The spatial resolution obtained using a pump-probe microscope is better than that obtained using a conventional fluorescence intensity microscope, because the pump-probe signal is based on the nonlinear interaction between the two laser beams and the sample due to the fact that the signal intensity is proportional to the product of the two [18]. We evaluated the spatial resolution in our setup by measuring the 20-nm gold nanoparticles dispersed on a glass slide as shown in Figs. 4(a) and 4(b). We used a 488-nm LD for the pump beam and a 532-nm DPSS for the probe beam. They were selected so that the wavelengths overlapped the absorption spectrum of the gold nanoparticles due to plasmon resonance with a peak at 524 nm. In this case, ground-state absorption bleaching and photothermal-induced light scattering may contribute to the measured signal [4, 19, 20]. To achieve the best resolution, we used a high numerical aperture (NA = 1.4) objective lens. Using the global fitting of a single particle with the Gaussian, the full width at half maximum (FWHM) values were calculated to be 142 ± 3 nm and 138 ± 3 nm in the transverse and vertical directions, respectively [Fig. 4(c)]. These values are substantially smaller than the calculated lateral FWHM value of the intensity distribution of a tightly focused probe beam waist under a diffraction-limited condition, w_{xy} ~0.51 λ/NA = 194 nm. The point-spreading function (PSF) produced by the pump-probe microscope is given by the product of the intensity distribution of the two beams at the focal point, and the lateral FWHM value is calculated as 132 nm, which is close to our experimental values. These results clearly demonstrate that sub-diffraction resolution imaging is achievable using our pump-probe microscopy, even for non-fluorescent species.

#206121 - $15.00 USD Received 7 Feb 2014; revised 26 Mar 2014; accepted 1 Apr 2014; published 7 Apr 2014

In the case of a fluorescent sample, it is possible to directly compare the conventional fluorescence-intensity image with the image created by the stimulated emission induced fluorescence intensity reduction (we call this method SEIFIR) in epifluorescence detection [7, 8]. The images of 1 μm fluorescence beads (Invitrogen TetraSpeck microspheres) obtained by measuring SEIFIR and fluorescence intensity are shown in Figs. 4(d) and 4(e), respectively. We used the 488-nm LD and the 532-nm DPSS as light sources for excitation and emission stimulation, respectively. The modulation frequencies of the former and the latter were set to 20 kHz and 33 kHz, respectively. We measured the SEIFIR and conventional-fluorescence images simultaneously, using a system comprised of the same detector and two lock-in amplifiers with demodulation set to the difference frequency (13 kHz) and the fundamental excitation frequency (20 kHz), respectively. Figure 4(f) shows the intensity profiles along the broken lines in Figs. 4(d) and 4(e). It is clear that SEIFIR microscopy improves spatial resolution.

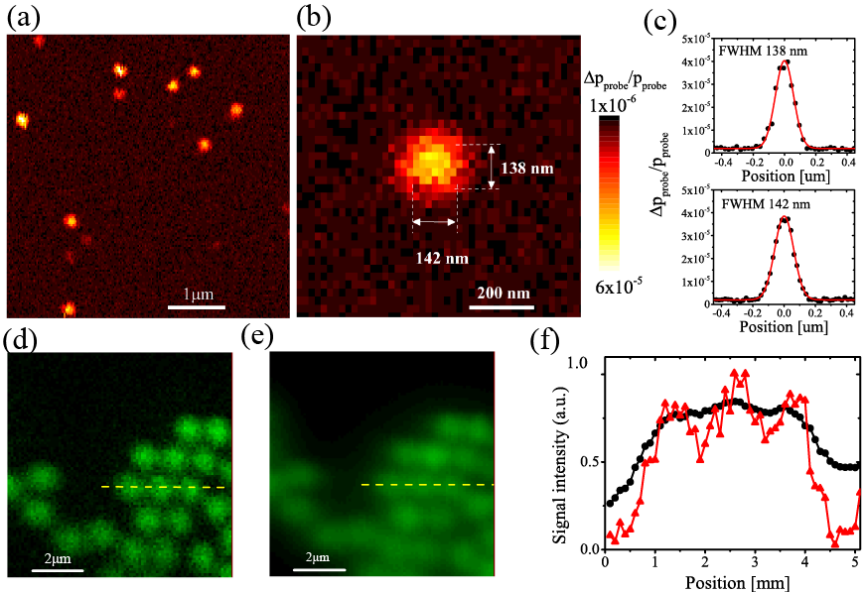

Fig. 4. Evaluation of spatial resolution in pump-probe microscopy. (a), (b) pump-probe images of 20 nm gold nanoparticles dispersed on a glass slide. (c) Intensity profiles of the single nanoparticle in the vertical and horizontal direction. The average power of the probe and pump beam was 115 and 222 μW, respectively. The modulation frequency of the pump and probe beams were 5.0 and 5.1 MHz, respectively. The time constant of the lock-in amplifier was 2 ms and the pixel dwell time was 6 ms. Global fitting of a single nanoparticle using the Gaussian results in full-width at half maximum of 138 nm and 142 nm in the vertical and transversal direction, respectively. Assuming the size of the nanoparticles to be 20 nm, deconvolution of the intensity profiles gives FWHMs of 136 nm and 140 nm for the effective PSF. (d), (e) Stimulated emission induced fluorescence intensity reduction (SEIFIR) image and conventional fluorescence intensity image of 1 μm fluorescence beads. The excitation and emission stimulation beams were focused by an objective lens with NA = 0.95. The average power of the excitation and emission stimulation beam was 23 μW and 1.1 mW, respectively. (f) Intensity profiles along the broken lines in (d) (red) and (e) (black).

2.5 Biological imaging

We demonstrated pump-probe imaging using biological samples. The stimulated-emission images of mouse CD8 T cells from the T-cell area of mesenteric lymph nodes, with and without the scheme of balanced detection are shown in Figs. 5(a) and 5(b), respectively. For preparing the sample, we removed mesenteric lymph-nodes from adult mice (C57BL/6 from Sankyo-Labo Service Corporation Inc., Tokyo, Japan), embedded the nodes in an OCT compound (Sakura Seiki, Tokyo, Japan), immersed them in liquid nitrogen to freeze them and

#206121 - $15.00 USD Received 7 Feb 2014; revised 26 Mar 2014; accepted 1 Apr 2014; published 7 Apr 2014

sliced them to 4-μm thickness. We stained the sections with an anti-CD8 antibody (S3-6.7 from eBioscience, CA), labelled them with eFluor 650NC (from eBioscience) and observed them under pump-probe microscopy. The antibody against CD8 was labelled with quantum dots, with the fluorescence peak at 650 nm. We were able to clearly visualize the cell structure using the balanced-detection scheme. Figure 5(c) shows the intensity profiles along the broken lines in Figs. 5(a) and 5(b). The relative background-fluctuation intensities in Figs. 5(a) and 5(b) were 1.3 x 10^{-6} and 9.8 x 10^{-6}, respectively.

Figure 5(d) shows a stimulated-emission image of an axon of a neuron in the cerebral cortex, expressing yellow fluorescent proteins. For preparing the sample, we fixed adult transgenic mice (two months old, thy1-GFP H-line, Jackson Lab.) by cardiac perfusion with PBS and paraformaldehyde, cut 100-μm slices of the frontal cortex using a vibratome (Leica VT1200) and embedded the slices in UNICRYL resin (Funakoshi Ltd.). To induce stimulated emission, we used a 488-nm LD for the pump and a 532-nm DPSS for the probe, so that the absorption and fluorescence spectra overlapped the wavelengths of the pump beam and the probe beam, respectively. These results suggest that our method has potential for the study of biological nanostructures and the functional properties of material such as brain tissue.

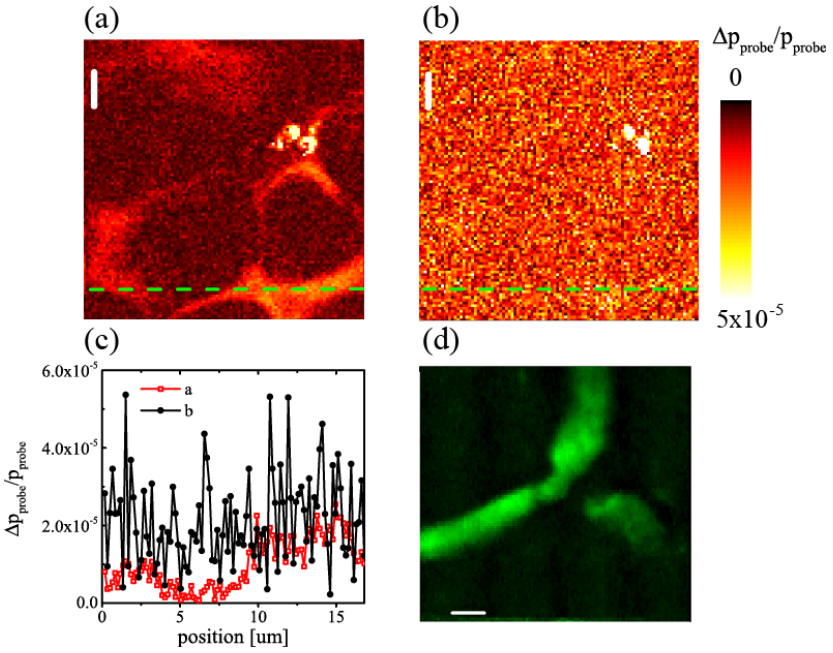

Fig. 5. (a), (b). Stimulated emission images of a mouse T cell labelled with quantum dots with and without the scheme of the balanced detection. We used 488 nm LD for the pump and 660 nm LD for the probe. The average powers of the probe and pump beam were 210 and 1 mW, respectively. The modulation frequency of the pump and probe beams were 3 and 3.1 MHz, respectively. The time constant of the lock-in amplifier was 5 ms and the pixel dwell time was 8 ms. (c). Intensity profiles along the broken lines in (a) (red) and (b) (black). (d) Stimulated emission image of neuron-expressing yellow fluorescent proteins. The average powers of the probe and pump beam were 130 μW and 970 μW, respectively. The scale bars in (a), (b) and (d) indicate 2 μm.

3. Discussion

In both the pulse and continuous wave laser systems, the ultimate SNR would be achieved when the pump beam intensity is enough to cause saturation and the probe beam intensity is close to saturation but not substantial saturation. Then imaging signal intensity is only limited by the shot noise of the probe beam. For the femtosecond pump-probe laser system, the detection limit of the relative intensity change of the probe beam is ~10^{-7} for 1-s time

#206121 - $15.00 USD Received 7 Feb 2014; revised 26 Mar 2014; accepted 1 Apr 2014; published 7 Apr 2014

constant at the lock-in amplifier [5], and this value is comparable to our continuous wave system

For ground state depletion, signal is proportional to the ground state absorption cross section, which is usually comparable to the stimulated emission cross section because of microscopic reversibility. Furthermore, if the excited state absorption cross section is of the same order of magnitude or larger than that of the ground state, even higher SNR signal can be expected. Because of the higher density of states in the higher electronic states, which can be the final states of the induced absorption signal, there is high possibility of intense induced absorption appearing in the available spectral range of diode laser. Therefore, if it is possible to select the wavelength in some probe molecular systems appropriate for the probe beam, our method is expected to be applicable to excited-state absorption and ground state absorption bleaching in addition to stimulated emission all at the same time allowing the multi-color imaging.

During the sample scanning, the non-uniformity of the refractive-index and stationary absorption in the sample caused the probe beam to vary in intensity due to inevitable non-uniform concentration and various component species, which led to an imbalance in intensity between the signal and the reference path. In our experimental setup, this intensity imbalance was cancelled out by the auto-gain controller with which the detector is equipped. This controller automatically adjusts the gain so that $g = \overline{p}_{\mathrm{sig}} / \overline{p}_{\mathrm{ref}}$, where $\overline{p}_{\mathrm{sig(ref)}}$ is the low-frequency component of the signal detected on the signal (reference) photodiode. To detect the lock-in signal while cancelling both the laser noise and the intensity imbalance during the sample scanning, we selected a bandwidth for the gain controller with a cut-off frequency higher than the inverse of the pixel-dwell time and lower than the lock-in frequency. We measured an image of transparent 1 μm polystyrene beads with a dwell time of 6 ms and confirmed that the refractive-index variations in the sample did not disturbed the lock-in signal.

Finally, we discuss the effect of the thermal lens on the measured signal because the thermal lens microscope is based on the same pump-probe detection scheme. When the excitation beam is absorbed, the temperature of the sample increases, forming a refractive index distribution that changes the divergence of the transmitted probe beam. Thermal lensing may contribute to the measured lock-in signal if the characteristic length of heat transport during one modulation period is larger than the wavelength of probe light, i.e., $d = \sqrt{2D / \omega_{1,2}} > \lambda_{\mathrm{probe}}$, where D is the thermal diffusivity (1.4 x 10^{-7} m^2/s in water). A typical characteristic of the thermal lens effect is that the signal intensity exhibits two peaks that correspond to focusing or defocusing when the sample position is moved in the axial direction [10, 21]. This becomes a drawback when the structures in the axial direction need to be resolved. To avoid thermal lens effect, we selected $\omega_{1,2}$ so that d was comparable or smaller than λ_{probe}. Furthermore, we used a condenser lens with an NA that was larger or equal to the focusing lens. To examine thermal lens effect on the present setup, the signal intensity and phase dependences on the relative distance between the sample and the focal position of the probe beam were measured by moving the slides of thin film of quantum dots. We found that the amplitude of the lock-in signal exhibited only a single peak at the origin. Furthermore, the phase was nearly flat and did not exhibit the π shift at the origin. We also checked the frequency characteristics of the signals and found that the signal intensity was nearly independent of the pump and probe modulation frequency in the range from 0.5 to 5 MHz. Therefore, we concluded that the thermal lens had negligible effects on the measured signal.

4. Conclusion

In conclusion, we have demonstrated that sub-diffraction resolution pump-probe imaging with shot-noise limited sensitivity can be carried out using conventional laser diodes with a balanced-detection scheme. The cost of LD was 50 times lower than in the Ti:sapphire laser-based system. Furthermore, LD is maintenance free and power consumption and space occupied by the instruments were reduced in comparison with the mode-locked laser-based

#206121 - $15.00 USD Received 7 Feb 2014; revised 26 Mar 2014; accepted 1 Apr 2014; published 7 Apr 2014

system. Blue, red and near-infrared laser diodes are readily available, as they are widely used in optical disks and in optical communication. In recent years, tremendous advances have been made in green-emitting (500–532 nm) InGaN-based LD technology, achieving an output power of more than 100 mW [22, 23]. Furthermore, green to yellow (543–570 nm) LDs with ~3 mW power can be used at room temperature [24]. By incorporating these LDs, our method becomes applicable to various types of probe materials including low molecular weight organic molecules, fluorescent proteins, and quantum dots. Thus, this method offers new opportunities for studying the nanostructures and properties of biological tissues.

Acknowledgments

This study was financially supported by a joint research project at the Institute of Laser Engineering, Osaka University, under contract number B1-27.